ISSN 1070-3284, Russian Journal of Coordination Chemistry, 2021, Vol. 47, No. 3, pp. 165–173. © Pleiades Publishing, Ltd., 2021.
Russian Text © The Author(s), 2021, published in Koordinatsionnaya Khimiya, 2021, Vol. 47, No. 3, pp. 137–146.

Molecular Magnets Based on Mononuclear Aqua and Aqua-Chloro Lanthanide (Tb, Dy, Er, Yb) Complexes with Bipyridine

S. P. Petrosyants[a], *, K. A. Babeshkin[a], **, A. B. Ilyukhin[a], and N. N. Efimov[a]

[a] *Kurnakov Institute of General and Inorganic Chemistry, Russian Academy of Sciences, Moscow, Russia*

**e-mail: petros@igic.ras.ru*

***e-mail: bkonstantan@yandex.ru*

Received August 31, 2020; revised September 16, 2020; accepted September 17, 2020

Abstract—The complexes $[Tb(Bipy)_2(H_2O)_2Cl_2]Cl$ (**I**), $[Ln(Bipy)(H_2O)_6]Cl_3·2H_2O·0.5Bipy$ (Ln = Dy (**II**), Yb (**IV**)), $[Er(Bipy)_2(H_2O)_3Cl]Cl_2·2H_2O$ (**III**), and $[Yb(Bipy)(H_2O)_6]Cl_3$ (**V**) were prepared using salts $LnCl_3·6H_2O$ (Ln = Tb, Dy, Er, Yb) and 2,2'-bipyridine (Bipy). The structure of complex **V** was determined by X-ray diffraction (CIF file CCDC no. 2024688). Magnetic characteristics of the complexes indicate that the replacement of water molecules in the coordination sphere of aqua chlorides by bidentate Bipy ligand gives single-molecule magnets with significant barriers for magnetization reversal, especially in the case of ytterbium compound, $\Delta E/k_B([Yb(Bipy)(H_2O)_6]Cl_3·2H_2O·0.5Bipy) = 43$ K.

Keywords: lanthanide chlorides, Bipy complexes, magnetism, single-molecule magnets

DOI: 10.1134/S1070328421030039

INTRODUCTION

Single-molecule magnets (SMMs) represent a modern alternative to traditional magnetic materials. Before the discovery of SMMs, nanoparticles were considered to be the smallest-size magnetic materials; currently, nanoparticles are widely known and studied in detail [1–4]. However, the advantage of SMMs over nanoparticles is not only their smaller size, but also the uniformity, relatively easy synthesis, and the possibility of varying magnetic properties by using different ligands in the design of molecular systems.

In the last decade, the greatest attention among SMMs has been attracted by lanthanide complexes [5–7]. It is for these compounds that the highest magnetization reversal barriers and blocking temperatures have now been attained [8–16]. These remarkable achievements are due to the large local anisotropy of heavy (starting from Tb) lanthanide ions. The magnetic anisotropy and high large magnetic moments make the synthesis and magnetic investigations of mononuclear lanthanide complexes a promising line of research [17–19]. However, prediction of properties of lanthanide-based SMMs is still a challenge. Recent studies show that the magnetic behavior of 4*f*-SMMs is very sensitive to their structural details, ligand field effects, and the presence and strength of intra- and intermolecular magnetic interactions. In particular, correlations between the coordination environment and magnetic relaxation of 4*f*-SMMs were recently found for Dy, Er, and Yb complexes with 2,2'-bipyridine (Bipy) and 1,10-phenanthroline (Phen) [20, 21].

For systematic study of the effect of the ligand composition on the magnetic relaxation of 4*f*-SMMs, here we synthesized mononuclear chloride complexes with bidentate heterocyclic Bipy ligand: $[Tb(Bipy)_2(H_2O)_2Cl_2]Cl$ (**I**), $[Ln(Bipy)(H_2O)_6]Cl_3·2H_2O·0.5Bipy$ (Ln = Dy (**II**), Yb (**IV**)), $[Er(Bipy)_2(H_2O)_3Cl]Cl_2·2H_2O$ (**III**), and $[Yb(Bipy)(H_2O)_6]Cl_3$ (**V**). The purity of the products was confirmed by powder X-ray diffraction, and the magnetic behavior of all complexes was investigated by static and dynamic magnetic susceptibility measurements.

EXPERIMENTAL

Commercial $LnCl_3·6H_2O$ (Ln = Tb, Dy, Er, Yb), Bipy (Aldrich), CH_3OH, C_2H_5OH, and $(C_2H_5)_2O$ were used as received. All operations were carried out in air.

Synthesis of $[Tb(Bipy)_2(H_2O)_2Cl_2]Cl$ (I). A solution of Bipy (0.156 g, 1.00 mmol) in C_2H_5OH (15 mL) was added to a solution of $TbCl_3·6H_2O$ (0.181 g, 0.484 mmol) in C_2H_5OH (15 mL) heated to $T \approx 40$°C. The mixture was stirred until it cooled down to room temperature. The homogeneous solution was transferred to an evaporation bowl; after a week of isothermal evaporation, the resulting phase was separated on a filter and washed with C_2H_5OH. The yield was 0.208 g (70% based on Tb). According to powder X-ray diffraction, the product was a mixture of phases **I** and $[Tb(H_2O)_3(Bipy)_2Cl]Cl_2·2H_2O$ (Fig. S1).

Synthesis of $[Dy(Bipy)(H_2O)_6]Cl_3 \cdot 2H_2O \cdot 0.5Bipy$ (II). A solution of $DyCl_3 \cdot 6H_2O$ (0.191 g, 0.506 mmol) in CH_3OH (15 mL) was added to a solution of Bipy (0.260 g, 1.66 mmol) in CH_3OH (10 mL). The resulting viscous mass was covered with $(C_2H_5)_2O$ and triturated up to formation of a crystalline phase, which was dried in air. The yield was 0.273 g (84% based on Dy). The single-phase nature of the product was confirmed by powder X-ray diffraction (Fig. S2).

For $C_{15}H_{28}N_3O_8Cl_3Dy$ (M = 647.256)

Anal. calcd., %	C, 27.83	H, 4.36	N, 6.49
Found, %	C, 27.45	H, 4.36	N, 5.99

Synthesis of $[Er(Bipy)_2(H_2O)_3Cl]Cl_2 \cdot 2H_2O$ (III). A solution of $ErCl_3 \cdot 6H_2O$ (0.191 g, 0.500 mmol) in C_2H_5OH (15 mL) was added to a solution of Bipy (0.160 g, 1.017 mmol) in C_2H_5OH (20 mL) heated to $T \approx 40$°C. The mixture was stirred until it cooled down to room temperature. The homogeneous solution was transferred to an evaporation bowl; after a week of isothermal evaporation, the resulting phase was separated on a filter and washed with C_2H_5OH. The yield was 0.264 g (78% based on Er). The single-phase nature of the product was confirmed by powder X-ray diffraction (Fig. S3).

For $C_{20}H_{26}N_4O_5Cl_3Er$ (M = 676.062)

Anal. calcd., %	C, 35.53	H, 3.88	N, 8.28
Found, %	C, 35.45	H, 4.30	N, 7.95

Synthesis of $[Yb(Bipy)(H_2O)_6]Cl_3 \cdot 2H_2O \cdot 0.5Bipy$ (IV). A solution of $YbCl_3 \cdot 6H_2O$ (0.193 g, 0.498 mmol) in C_2H_5OH (15 mL) was added to a solution of Bipy (0.154 g, 0.984 mmol) in C_2H_5OH (10 mL), and the mixture was stirred for 30 min. The resulting viscous material was worked-up as in the synthesis of **II**. The yield was 0.273 g (84% based on Yb). The single-phase nature of the product was confirmed by powder X-ray diffraction (Fig. S4).

For $C_{15}H_{28}N_3O_8Cl_3Yb$ (M = 657.796)

Anal. calcd., %	C, 27.39	H, 4.29	N, 6.38
Found, %	C, 27.45	H, 4.36	N, 5.95

The single crystals of **$[Yb(Bipy)(H_2O)_6]Cl_3$ (V)** were isolated from an ethanol solution containing $YbCl_3 \cdot 6H_2O$ and Bipy (1 : 2 ratio).

Elemental analysis was carried out by standard procedures using a EUROEA 3000 CHN analyzer. Powder X-ray diffraction analysis was performed on a Bruker D8 Advance diffractometer (CuK_α, Ni filter, LYNXEYE detector, reflection geometry). The full-profile Rietveld refinement of the structures of **II**, **III**, and **IV** was done with the TOPAS program [22] (Figs. S2–S4, Table 1).

X-ray diffraction study of compound **V** was carried out on a Bruker SMART APEX2 diffractometer (MoK_α radiation, λ = 0.71073 Å, graphite monochromator) [23]. The absorption corrections were applied by the semiempirical method based on equivalents using the SADABS program [24]. The structure was solved by a combination of direct methods and Fourier maps and refined by full-matrix anisotropic-isotropic least squares calculations. The positions of H atoms of Bipy were calculated from geometric considerations and refined by the riding model, while H atom positions of H_2O molecules were located from Fourier maps and refined using restraints (DFIX 0.90 0.03). All calculations were carried out by SHELXS and SHELXL program packages [25]. Selected crystallographic data and results of structure refinement for **V** are summarized in Table 2.

Experimental data for the structure of **V** were deposited with the Cambridge Crystallographic Data Centre (CCDC no. 2024688; deposit@ccdc.cam.ac.uk or http://www.ccdc.cam.ac.uk/data_request/cif).

The magnetic behavior of complexes **II**–**IV** was investigated by static and dynamic magnetic susceptibility measurements on a PPMS-9 magnetometer (QuantumDesign) in the temperature range of 2–300 K in static magnetic fields of 0–5000 Oe. The dynamic magnetic susceptibility was measured using alternating magnetic fields with strengths of 5, 3, and 1 Oe for alternating field frequency ranges of 10–100, 100–1000, and 10–10000 Hz, respectively. With these measurement conditions, it was possible to avoid heating of the sample at low temperatures (this can occur at high amplitude and modulation frequency) and to obtain the best signal-to-noise ratio. All magnetic behavior measurements were carried out for ground polycrystalline samples sealed in plastic bags and frozen in mineral oil to prevent the orientation of crystallites in a magnetic field [26]. The paramagnetic component of the magnetic susceptibility (χ) was determined considering the diamagnetic contribution of the sample, estimated from the Pascal constant, and diamagnetic contributions of mineral oil and the holder.

RESULTS AND DISCUSSION

The synthesis of coordination compounds using hydrated salts as the starting materials is often carried out in mixed water–alcohol solvation systems; this accounts for the diversity of isolated products. In the case of Bipy ligand, the product composition depends also on the ligand to central atom ratio. The isolated compounds can contain different amounts of the bidentate ligand, chloride ions, and water molecules in the inner and outer coordination spheres [27]. As a result, it is necessary to select conditions for each

Table 1. Results of structure refinement for compounds **II**–**IV**

Parameter	Value		
	II	**III**	**IV**
System	Triclinic	Monoclinic	Triclinic
Space group	$P\bar{1}$	$P2_1/n$	$P\bar{1}$
a, Å	11.6696(13)	17.3380(19)	11.66197(50)
b, Å	10.909(6)	9.2085(12)	10.94937(35)
c, Å	10.1771(6)	17.2682(15)	10.08126(38)
α, deg	86.072(8)	90	85.7694(25)
β, deg	74.814(8)	117.3185(63)	74.6135(28)
γ, deg	79.626(7)	90	79.5111(30)
V, Å^3	1229.59(18)	2449.52(49)	1219.970(82)
Z	2	4	2
Range of 2θ, deg	5–50	5–50	5–50
Step of 2θ, deg	0.02	0.02	0.02
R_{cryst}	1.38	3.16	3.74
R_{wp}	5.31	4.08	5.49
R_p	3.50	3.05	4.11
GOOF	3.86	1.29	1.47

complex-forming agent in order to obtain a pure sample (according to powder X-ray diffraction data). For example, the synthesis of complex **IV** (XEWWUR [28]) is described for Bipy : Yb ≈ 2, and an increase in the Bipy : Yb molar ratio to 3 also resulted in the formation of pure XEWWUR. Complex **IV** was also present in other syntheses using 95% C_2H_5OH, variable temperature, and different orders of reactant mixing, but complex $[Yb(Bipy)_2(H_2O)Cl_2]Cl$ was formed together with XEWWUR [28].

Compounds **II**–**IV** were single phases (Fig. S2–S4, Table 1). In all compounds, the Ln coordination number is 8, and the coordination polyhedron resembles most closely a two-capped trigonal prism (**II**, **IV**; Fig. 1a) and a square antiprism (**III**; Fig. 1b). The powder X-ray diffraction study of the product obtained in the synthesis of compound **I** showed that the sample was not a single phase (Fig. S1), but contained ~10% of $[Tb(Bipy)_2(H_2O)_3Cl]Cl_2{\cdot}H_2O$ (EPUPUC, [29]). No single-phase product was obtained in the synthesis of **I** under any conditions.

We isolated single-crystalline product **V** from a solution of $YbCl_3{\cdot}6H_2O$ and Bipy (1 : 2 ratio) in C_2H_5OH and studied it by X-ray diffraction (Table 2). This structure was known previously [28]; however, the single crystal X-ray diffraction pattern of **V** that we

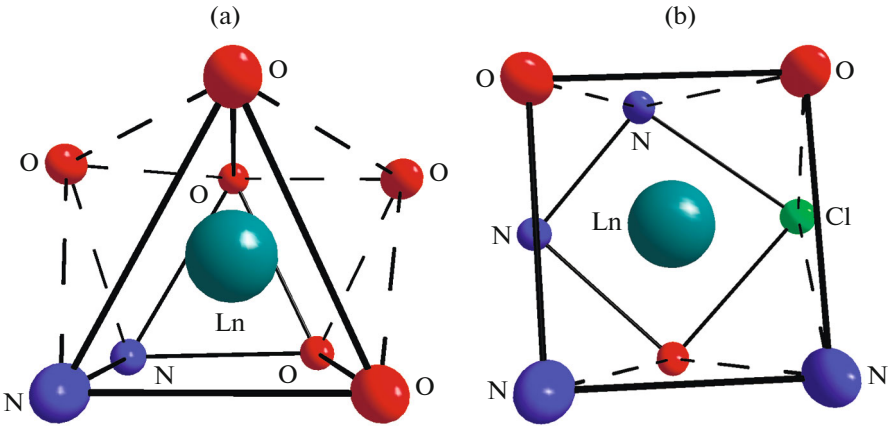

Fig. 1. Coordination polyhedra of lanthanides for compounds (a) **II** and **IV**; (b) **III**.

Table 2. Selected crystallographic data and results of structure refinement for compound **V**

Parameter	Value
M	543.67
T, K	150(2)
System	Monoclinic
Space group	$P2_1/n$
a, Å	14.2178(5)
b, Å	7.6379(3)
c, Å	17.3344(6)
β, deg	90.8530(10)
V, Å^3	1882.21(12)
Z	4
ρ(calcd.), g/cm^3	1.919
μ, mm^{-1}	5.418
F(000)	1052
Sample size, mm	0.2 × 0.18 × 0.06
Range of θ, deg	2.350–29.578
Ranges of h, k, l	$-19 \le h \le 16$, $-10 \le k \le 10$, $-23 \le l \le 23$
Number of measured reflections	17310
Number of unique reflections (R_{int})	4957 (0.0394)
Completeness to θ = 25.242°, %	99.9
Max, min transmission	0.4929, 0.38
Number of parameters	236
S	1.000
R_1, wR_2 ($I > 2\sigma(I)$)	0.0293, 0.0610
R_1, wR_2 (all data)	0.0532, 0.0684
$\Delta\rho_{max}/\Delta\rho_{min}$, e/Å^3	1.733/–0.750

obtained was of much higher quality than that reported in the literature, in particular, the unit cell parameters were determined with a higher accuracy.

The magnetic properties of all obtained complexes were investigated in the 2–300 K range in a 5000 Oe external magnetic field (Fig. 2). The $\chi_m T(T)$ curves for complexes **II** and **III** are similar. During cooling from room temperature to 2 K, the $\chi_m T$ values barely change over a broad temperature range, down to 85 K (**II**) and 100 K (**III**), and then gradully decrease down to 5 K. During further cooling, the $\chi_m T$ values decrease more sharply to reach a minimum at 2 K. In the case of Yb complex **IV**, the $\chi_m T$ values decrease with decreasing temperature at approximately the same rate over the whole temperature range.

The shape of the $\chi_m T(T)$ curve for all complexes corresponds to that for mononuclear complexes of the same lanthanides [30], while $\chi_m T$ (300 K) values for **II**–**IV** are in satisfactory agreement with the theoretical values for isolated Ln^{3+} ions (Table 3). In view of rather long (>6.5 Å) Ln...Ln distances in **II**–**IV**, the nature of the Ln^{3+} ions appears to have a crucial effect on the magnetic behavior of the complexes.

Quite a few complexes of heavy lanthanides demonstrate slow relaxation of magnetization. In order to check the presence of slow magnetic relaxation, the dynamic magnetic susceptibility was studied for all complexes obtained in this work. These measurements gave the frequency dependences of the real (χ') and imaginary (χ") components of the magnetic susceptibility in up to 5000 Oe magnetic fields at 2 K.

In zero magnetic field, a pronounced signal in the χ"(ν) curve is observed only for complex **II**. However, the maximum is located outside the frequency range of the equipment, which precludes determination of the parameters of slow magnetic relaxation. For all other complexes, the deviations of the χ"(ν) curves from zero are within the error of measurement of the

magnetometer. In order to reduce the possible effect of quantum tunneling of magnetization (QTM), which may increase the relaxation rate, the $\chi''(\nu)$ values of compounds **II**–**IV** were measured in external magnetic fields of various strength up to 5000 Oe (Fig. S5–S7).

The application of external magnetic field made it possible to detect and study the slow magnetic relaxation for all of the compounds. The optimal magnetic field corresponding to the longest relaxation time is 1000 Oe for all complexes (Figs. S5–S7). The frequency dependences of real (Fig. S8) and imaginary (Fig. 3) components of magnetic susceptibility were measured in various temperature ranges in the optimal magnetic field. The approximation of $\chi''(\nu)$ isotherms using the generalized Debye model gave dependences of the relaxation time on the reciprocal temperature $\tau(1/T)$ (Fig. 4).

The $\chi''(\nu)$ curves of compound **II** exhibit two peaks (Fig. 3a); one peak is beyond the right boundary of the frequency range of the instrument even at 5 K (high-frequency peak), whereas the second, less intense, peak can be recorded down to 7 K (low-frequency peak). The presence of two peaks in the frequency dependences of the imaginary magnetic susceptibility was previously described for mononuclear SMMs [31–36]. This could be attributed to polymorphism [37], which fundamentally changes the properties of the single-molecule magnet. However, the X-ray diffraction pattern of **II** shows no signs of a second phase. The appearance of a second peak in $\chi''(\nu)$ could also be due to intra- or intermolecular interaction between lanthanide ions [38]. However, the minimum Dy–Dy distance is 6.78 Å, which rules out the intermolecular magnetic interaction. Thus, the presence of two peaks is likely to be due to disorder of the hydrogen ion in the coordinated water molecule, as in the previously studied benchrotrenecarboxylic acid derivatives [39]. One more possible explanation is appearance of the second relaxation peak due to the magnetic dipole–dipole interaction [40]. The relaxation parameters were determined for both observed relaxation processes.

For determining the relaxation parameters of the obtained compounds, high-temperature regions (Table 4) of the $\tau(1/T)$ curves were approximated by the Arrhenius equation describing the Orbach relaxation mechanism

$$\tau_{Or}^{-1} = \tau_0^{-1}\exp(-\Delta E/k_BT),$$

where $\Delta E/k_B$ is the height of the energy barrier for magnetization reversal of the molecule; k_B is the Boltzmann constant, τ_0 is the shortest relaxation time, T is temperature. The optimal agreement between theoretical dependences and experimental data for the same temperature ranges was attained using the sets of parameters of complexes **II**–**IV** summarized in Table 4. For all of the obtained complexes exhibiting slow magnetic relaxation, the dependences $\tau(1/T)$

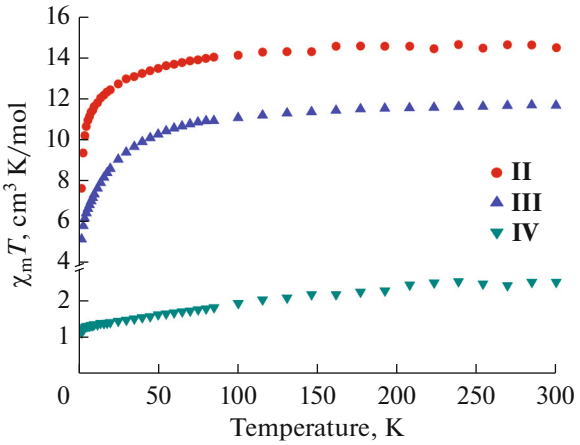

Fig. 2. Temperature dependences $\chi_m T(T)$ of compounds **II**–**IV** in a 5000 Oe static magnetic field.

deviate from linearity (Fig. 4). Apparently, other mechanisms are also involved in the relaxation of magnetization; if these mechanisms are known, it will be possible to derive a complete relaxation equation for each complex.

The best approximation of the experimental $\tau(1/T)$ data for complexes **II** (low-frequency peak) and **IV**, exhibiting slow magnetic relaxation, was attained by using the sum of the Orbach and Raman relaxation mechanisms ($\tau_{Ram}^{-1} = C_{Ram}T^{nRam}$), where C_{Ram} and n_{Ram} are Raman relaxation parameters. For approximation of the whole body of experimental data for the high-frequency peak of complexes **II** and **III**, the sum of the Raman and QTM relaxation processes is optimal ($\tau_{KTH}^{-1} = B_{QTM}$). The best approximation of the theoretical dependence to the experimental data was found in all cases using the relaxation parameters presented in Table 4. The use of other relaxation mechanisms and their sums led to insufficiently good agreement between the experimental data and the theoretical curve and/or to excessive parameterization. From the results of measurements, it can be seen that compounds **II**–**IV** behave as single-molecule magnets in an external magnetic field.

Table 3. Experimental* and theoretical $\chi_m T$ values for isolated Ln^{3+} ions

Compound	$\chi_m T$ (300 K)	$\chi_m T$ (theor.)	$\chi_m T$ (2 K)
	cm^3 K/mol		
I	11.89	11.82	6.51
II	14.46	14.17	7.63
III	11.66	11.48	5.16
IV	2.54	2.57	1.12

* Static field of 5000 Oe.

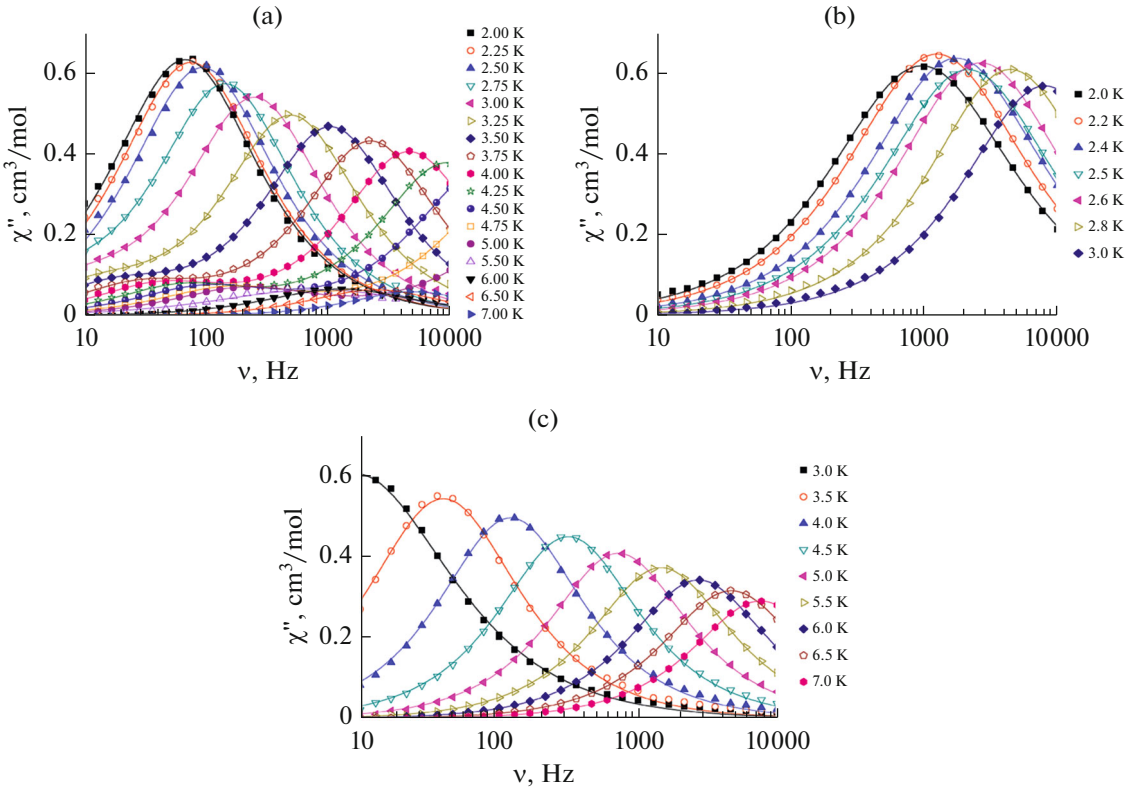

Fig. 3. Frequency dependences of the imaginary dynamic magnetic susceptibility of complexes (a) **II**, (b) **III**, and (c) **IV** in a 1000 Oe magnetic field (the lines show the approximation using the generalized Debye model).

The possibility of a contribution of quantum tunneling to the relaxation of magnetization of molecular systems in an external magnetic field has not yet been ultimately clarified. In a zero magnetic field, the QTM is often the major mechanism of magnetic relaxation. It is believed that the QTM can be completely suppressed by application of a magnetic field of the optimal strength. In some studies devoted to slow magnetic relaxation of Dy complexes, the authors claimed that in optimal magnetic fields, the QTM is completely eliminated [41, 42]. However, other researchers stated that for some compounds, the QTM cannot be completely suppressed despite the application of an external static magnetic field. For example, the absence of slow relaxation for a Er complex, was attributed exactly to the substantial effect of QTM [43]. Also, it was shown [44] that the QTM effect is present even in a 2000 Oe field. Furthermore, in [45], like for complex **II**, several peaks were observed in the χ"(ν) curve in a 1500 Oe static magnetic field, which were also interpreted as two different relaxation processes. The authors approximated one of the relaxation processes by the sum of the Orbach and QTM relaxation mechanisms. A more detailed discussion of the most realistic relaxation pathways makes sense if quantum chemical data on the probability of particular mechanisms are available.

For lanthanide complexes with bulky N-donor ligands such as Bipy, the barrier for magnetization reversal of complex **III** is fairly high. Indeed, $\Delta E/k_B$ of complex **III** (20 K) is lower than $\Delta E/k_B$ of $[HBipy][Er(Bipy)_2(NCS)_4]\cdot H_2O$ (35 K) [21]. According to [21, 46–48], the most probable reason is that the square antiprism is a more promising polyhedron for slow magnetic relaxation and for SMM behavior of Er complexes than a two-capped trigonal prism (Fig. 1a). Also, in the case of Er complexes, a significant factor is uniformity of the coordination environment, which is not attained in **III**, as it contains two sorts of donor centers: O and N.

It was shown [21, 49–51] that an increase in the number of types of atoms in the Yb coordination polyhedron leads to increasing barrier for magnetization reversal (ΔE). The Yb coordination polyhedron exhibiting a record-high ΔE value among Yb containing SMMs is a square antiprism, which is present in the obtained complex **IV** (Fig. 1b). This accounts for the fact that the barrier for magnetization reversal of **IV** ($\Delta E/k_B = 43$ K) approaches those of dysprosium complexes (for this class of compounds) and is currently one of the highest known values for ytterbium compounds [21].

Additionally, the coordination environment and, hence, the magnetic properties can be affected by the

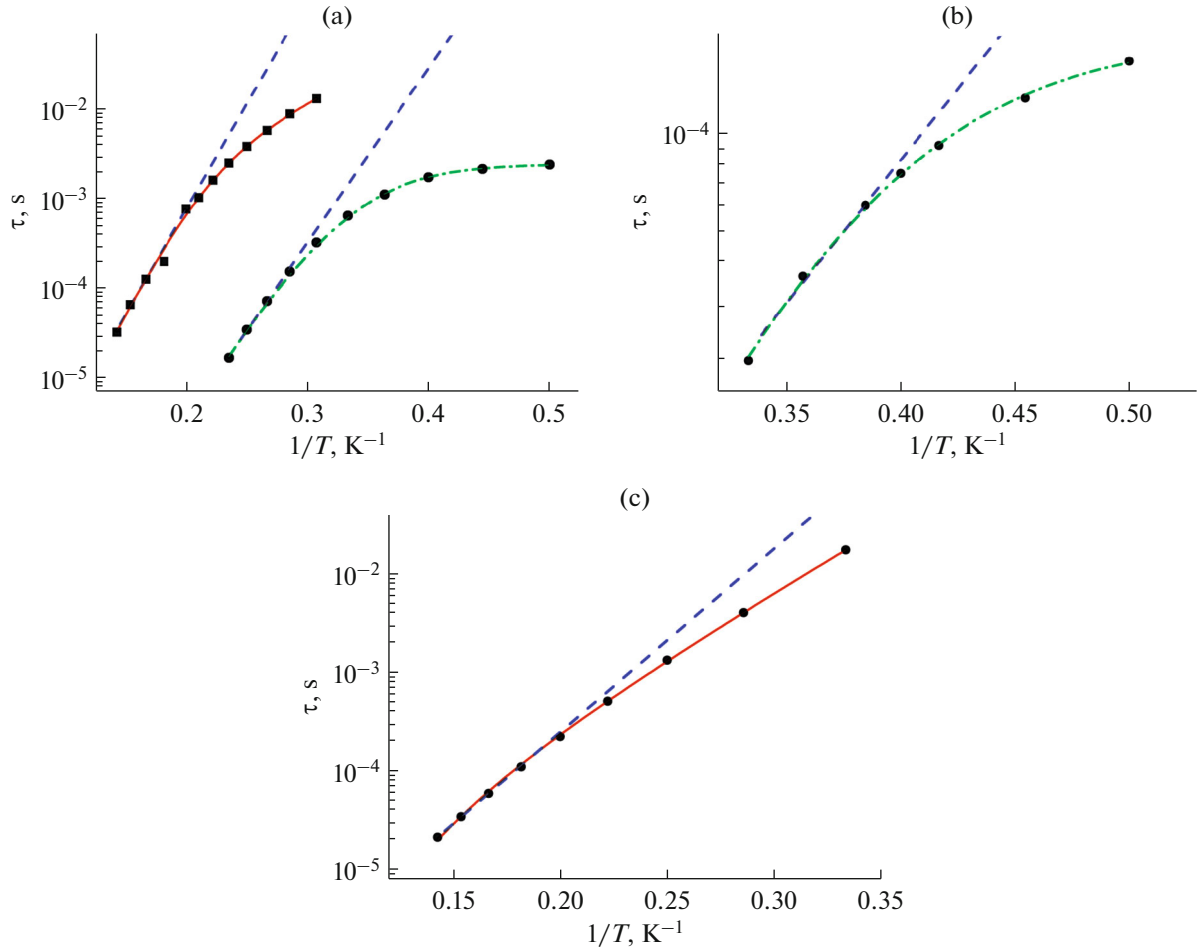

Fig. 4. Relaxation times of complexes: (a) **II** (squares are low-frequency peak; circles are high-frequency peak), (b) **III**, and (c) **IV** in a 1000 Oe magnetic field vs. reciprocal temperature. The dashed lines show the approximation of high-temperature regions using the Orbach mechanism; the continuous lines show the approximation using the sum of the Orbach and Raman mechanisms; the dash-and-dot lines show the approximation using the sum of the Raman and QTM mechanisms.

crystal packing, the presence of hydrogen bonds, and stacking interactions in the complexes [37, 52]. Only hydrogen bonds between the chlorine atoms in the lanthanide coordination environment and the hydrogen ions of coordinated water molecules are present in compound **III**, giving rise to a branched 3D structure. In the case of compounds **II** and **IV**, stacking interactions and Cl–H hydrogen bonds act cooperatively. This also gives rise a 3D structure containing parallel planes that accommodate all coordinated Bipy molecules. This ordering of complex ions additionally anchors their coordination environment, which may have an adverse effect on the SMM properties.

The performed studies provide the conclusion that compounds **II**–**IV** behave as field-induced single-molecule magnets. Complex **II** exhibits two relaxation processes, which may be due to either disorder of the hydrogen ions of coordinated water molecules or magnetic dipole–dipole interactions. Complex **IV** has a barrier for magnetization reversal comparable with the record-high values for this class of lanthanide complexes. In addition, the previously reported [21] empirical dependences of the barrier for magnetization reversal on the type and relative positions of donor centers were confirmed.

ACKNOWLEDGMENTS

The study was carried out using the research equipment of the Center for Collective Use of Physical Investigation Methods of the Kurnakov Institute of General and Inorganic Chemistry, Russian Academy of Sciences.

FUNDING

The synthesis and investigation of complexes **I** and **II** were supported by the Russian Science Foundation (grant no. 16-13-10407); the synthesis and investigation of complexes **III** and **IV** were supported by the Russian Foundation for Basic Research (grant no. 18-33-20155). Elemental analysis was performed within the state assignment for the

Table 4. Results of approximation of dependences $\tau(1/T)$ for complexes **II**–**IV**

Complex		**II** (high-frequency peak)	**I** (low-frequency peak)	**III**	**IV**
Figure		4a		4b	4c
Orbach	Temperature range, K	6–7		2.6–3	6–7
	$\Delta E/k_B$, K	45	54	20	43
	τ_0, s	4.0×10^{-10}	1.5×10^{-8}	2.3×10^{-8}	1.7×10^{-8}
Orbach + Raman	Temperature range, K	2–7		2–3	3–7
	C, $K^{-n_{Raman}} s^{-1}$		0.18		8.6×10^{-4}
	n_{Raman}		5.1		9.0
	$\Delta E/k_B$, K		60		31
	τ_0, s		7.2×10^{-9}		7.0×10^{-7}
Raman + QTM	Temperature range, K	2–7		2–3	3–7
	C, $K^{-n_{Raman}} s^{-1}$	7.0×10^{-3}		2.26	
	n_{Raman}	11		9	
	B_{QTM}	412		4945	

Kurnakov Institute of General and Inorganic Chemistry, Russian Academy of Sciences.

CONFLICT OF INTEREST

The authors declare that they have no conflicts of interest.

SUPPLEMENTARY INFORMATION

The online version contains supplementary material available at https://doi.org/10.1134/S1070328421030039.

REFERENCES

1. Gatteschi, D., Villain, J., and Sessoli, R., *Molecular Nanomagnets*, Oxford: Oxford University, 2006.
2. Winpenny, R. and Aromí, G., *Single-Molecule Magnets and Related Phenomena*, Springer, 2006.
3. Bartolomé, S.J., Luis, F., and Fernandez, J.F., *Molecular Magnets: Physics and Applications*, Springer, 2014.
4. Benelli, C. and Gatteschi, D., *Introduction to Molecular Magnetism: From Transition Metals to Lanthanides*, Wiley, 2015.
5. Layfield, R.A. and Murugesu, M., *Lanthanides and Actinides in Molecular Magnetism*, Wiley-VCH, 2015.
6. Gupta, S.K. and Murugavel, R., *Chem. Commun.*, 2018, vol. 54, p. 3685.
7. Feng, M. and Tong, M.-L., *Chem.-Eur. J.*, 2018, vol. 24, p. 7574.
8. Guo, F.-S., Day, B.M., Chen, Y.-C., et al., *Angew. Chem., Int. Ed. Engl.*, 2017, vol. 56, p. 11445.
9. Guo, F.S., Day, B.M., Chen, Y.-C., et al., *Angew. Chem.*, 2017, vol. 129, p. 11603.
10. Goodwin, C.A.P., Ortu, F., Reta, D., et al., *Nature*, 2017, vol. 548, p. 439.
11. Woodruff, D.N., Winpenny, R.E., and Layfield, R.A., *Chem. Rev.*, 2013, vol. 113, p. 5110.
12. Zhang, P., Zhang, L., and Tang, J., *Dalton Trans.*, 2015, vol. 44, p. 3923.
13. Lee, S. and Ogawa, T., *Chem. Lett.*, 2017, vol. 46, p. 10.
14. Lu, J., Guo, M., and Tang, J., *Chem. Asian J.*, 2017, vol. 12, p. 2772.
15. McAdams, S.G., Ariciu, A.-M., Kostopoulos, A.K., et al., *Coord. Chem. Rev.*, 2017, vol. 346, p. 216.
16. Guo, F.-S., Day, B.M., Chen, Y.C., et al., *Science*, 2018, vol. 362, p. 1400.
17. Sessoli, R. and Powell, A.K., *Coord. Chem. Rev.*, 2009, vol. 253, p. 2328.
18. Sorace, L., Benelli, C., and Gatteschi, D., *Chem. Soc. Rev.*, 2011, vol. 40, p. 3092.
19. Guo, Y.-N., Ungur, L., Granroth, G.E., et al., *Sci. Rep.*, 2014, vol. 4, p. 5471.
20. Petrosyants, S.P., Dobrokhotova, Zh.V., Ilyukhin, A.B., et al., *Eur. J. Inorg. Chem.*, 2017, p. 3561.
21. Petrosyants, S.P., Babeshkin, K.A., Gavrikov, A.V., et al., *Dalton Trans.*, 2019, vol. 48, p. 12644.
22. *TOPAS*, Karlsruhe (Germany): Bruker AXS, 2005.
23. *APEX II and SAINT*, Madison: Bruker AXS Inc., 2007.
24. Sheldrick, G.M., *SADABS*, Göttingen: Univ. of Göttingen, 1997.
25. Sheldrick, G.M., *Acta Crystallogr., Sect. C: Struct. Chem.*, 2015, vol. 71, no. 1, p. 3.
26. Petrosyants, S.P., Ilyukhin, A.B., Efimov, N.N., and Novotortsev, V.M., *Russ. J. Coord. Chem.*, 2018, vol. 44, no. 11, p. 660. https://doi.org/10.1134/S1070328418110064

27. Petrosyants, S.P., *Russ. J. Coord. Chem.*, 2019, vol. 45, no. 11, p. 749.
28. Semenova, L.I., Skelton, B.W., and White, A.H., *Aust. J. Chem.*, 1999, vol. 52, no. 6, p. 551.
29. Puntus, L.N., Lyssenko, K.A., Pekareva, I.S., and Bunzli, J.-G., *J. Phys. Chem. B*, 2009, vol. 113, p. 9265.
30. Kahn, O., *Molecular Magnetism*, New York: VCH, 1993.
31. Pinkowicz, D., Ren, M., Zheng, L.-M., et al., *Chem.-Eur. J.*, 2014, vol. 20, p. 12502.
32. Gupta, S.K., Rajeshkumar, T., Rajaraman, G., and Murugavel, R., *Chem. Commun.*, 2016, vol. 52, p. 7168.
33. Habib, F., Luca, O.R., Vieru, V., et al., *Angew. Chem., Int. Ed. Engl.*, 2013, vol. 52, p. 11290.
34. Jeletic, M., Lin, P.H., Le Roy, J.J., et al., *J. Am. Chem. Soc.*, 2011, vol. 133, p. 19286.
35. Lucaccini, E., Briganti, M., Perfetti, M., et al., *Chem.-Eur. J.*, 2016, vol. 22 P, p. 5552.
36. Ruiz, J., Mota, A.J., Rodríguez-Diéguez, A., et al., *Chem. Commun.*, 2012, vol. 48, p. 7916.
37. Pavlov, A.A., Nelyubina, Y.V., Kats, S.V., et al., *J. Phys. Chem. Lett.*, 2016, vol. 7, no. 20, p. 4111.
38. Hu, Z.-B., Jing, Z.-Y., Li, M.-M., et al., *Inorg. Chem.*, 2018, vol. 57, p. 10761.
39. Gavrikov, A.V., Koroteev, P.S., Efimov, N.N., et al., *Dalton Trans.*, 2017, vol. 46, p. 3369.
40. Li, J., Han, Y., Cao, F., et al., *Dalton Trans.*, 2016, vol. 45, p. 9279.
41. Yang, L., Wang, X., Zhu, M., et al., *Inorg. Chem. Front.*, 2019, vol. 6, p. 2142.
42. Zhang, S., Mo, W., Yin, B., et al., *Dalton Trans.*, 2018, vol. 47, p. 12393.
43. Liu, C., Li, M., Zhang, Y., et al., *Eur. J. Inorg. Chem.*, 2019, vol. 24, p. 2940.
44. Wang, R., Wang, H., Wang, J., et al., *CrystEngComm*, 2020, vol. 22, p. 2998.
45. Katoh, K., Yasuda, N., Damjanović, M., et al., *Chem. A Eur. J.*, 2020, vol. 26, p. 4805.
46. Gonzalez, J.F., Montigaud, V., Saleh, N., et al., *Magnetochemistry*, 2018, vol. 4, p. 39.
47. Lim, K.S., Kang, D.W., Song, J.H., et al., *Dalton Trans.*, 2017, vol. 46, p. 739.
48. Silva, M.R., Martín-Ramos, P., Coutinho, J.T., et al., *Dalton Trans.*, 2014, vol. 43, p. 6752.
49. Gavrikov, A.V., Efimov, N.N., Dobrokhotova, Zh.V., et al., *Dalton Trans.*, 2017, vol. 46, p. 11806.
50. Liu, J.-L., Yuan, K., Leng, J.-D., et al., *Inorg. Chem.*, 2012, vol. 51, p. 8538.
51. Soussi, K., Jung, J., Pointillart, F., et al., *Inorg. Chem. Front.*, 2015, vol. 2, p. 1105.
52. Kobayashi, F., Ohtani, R., Nakamura, M., et al., *Inorg. Chem.*, 2019, vol. 58, no. 11, p. 7409.

Translated by Z. Svitanko